JOURNAL OF SOLID STATE CHEMISTRY 46, 139–150 (1983)

On the Luminescence of Ions with s^2 Configuration in Lithium Hydride Crystals

S. O. CHOLAKH* AND G. BLASSE

Physical Laboratory, State University, P.O. Box 80.000, 3508 TA Utrecht, The Netherlands

Received June 9, 1982

The luminescence of the following ions with s^2 configuration was studied in lithium hydride (LiH) crystals: Ge^{2+}, Sn^{2+}, Sb^{3+}, Pb^{2+}, and Bi^{3+}. Their emission spectra show pronounced vibrational structure. These are discussed in terms of A_T and A_X emission with underlying trap levels. The temperature dependences of the decay times confirm such a model. The presence of more than one type of center and of lithium colloids prevents a complete analysis.

1. Introduction

The luminescence of alkali halide crystals doped with ions with s^2 configuration has been thoroughly investigated (*1*). Two emission bands can be observed in most phosphors after excitation into the A band. They are called A_T (higher energy) and A_X (lower energy). The adiabatic potential energy surface (APES) of the $^3T_{1u}$ relaxed excited state (RES) contains two minima (T and X). These arise from Jahn–Teller coupling of the orbital triplet to E_g and T_{2g} lattice modes (*2, 3*). The structure of the minima is complex, because trap levels exist below the T and X minima.

In MgO and CaO these ions show only A_T emission. This emission shows extended vibrational structure which has been studied by many authors (*4–6*).

Lithium hydride (LiH) has the same crystal structure (rock salt) as the host lattices mentioned above. Not much work on activators in LiH has been reported in the literature, probably due to the fact that single crystals are hard to prepare. Preliminary measurements on the luminescence of doped LiH single crystals have been reported in the literature by Rebane *et al.* (*7, 8*). These crystals, however, were of poor quality. Here we report on the luminescence of ions with s^2 configuration in LiH crystals of much better quality. The optical properties and luminescence of undoped crystals has been reported before (*9*). Our results show that the emission bands are highly structured. The luminescence of these ions in LiH is strikingly different from that observed in the alkali halide lattices.

2. Experimental

The LiH single crystals were grown in Urals Polytechnical Institute using a modification of the Stockbarger method (*10*). A

*On leave from Urals Polytechnical Institute, P.B. 620002, Sverdlovsk, USSR.

0022-4596/83/020139-12$03.00/0

steel tube and crucible remain stationary, whereas the furnaces were moving upward with a rate of 4 mm/hr. Three hot zone tube furnaces were used. During growth their temperatures are 750 (upper), 780 (center), and 670°C (lower). Lithium metal was vacuum distilled several times. The crucible was made of a special type of steel (ARMCO), which was selected upon reactivity with the lithium melt. The crucible had an inner diameter of 3.2 cm. The inner wall was highly polished and ended in a 90° cone.

The hydrogenation of lithium occurs at 710°C. Spectroscopically pure H_2 was used. The H_2 pressure was about 10 atm to decrease the dissociation of the LiH melt. Crystals were in the form of cylinders 5–6 cm long and 3 cm in diameter. They were slightly blue-colored due to colloidal lithium particles.

Doped crystals were prepared by using very pure metals (Ge, Sn, Sb, Pb, Bi). Plates cleaved from the crystal were annealed in hydrogen at 550°C for 80–100 hr to reduce internal tension and to improve stoichiometry.

The optical instrumentation was the same as used previously in other studies (*11*). It consists of a Perkin–Elmer spectrofluorimeter MPF-3 equipped with an Oxford helium cryostat.

3. Results

Before giving the more specific results the following general observations are presented. They should be kept in mind. All crystals show continuous absorption in the excitation as well as in the emission range of the luminescent centers under study. Since this absorption does not coincide with our excitation spectra, it must be due to one or more other centers which do not luminesce. Figure 1 gives a specific example of such an absorption spectrum. It will not be discussed any further in this paper. In spite of these complicating absorptions, the present study was undertaken since these crystals are the best we could obtain and, as far as we are aware, the best described in the literature up till now.

The emission spectra at LHeT can be divided in two groups, viz., relatively narrow emissions in which one-phonon lines dominate (Ge^{2+}, Sn^{2+}, Pb^{2+}) and broader emissions in which a progression in a certain frequency is observed (all cases). The former can be excited in the visible; the latter selectively in the uv. The excitation spectra consist of broad bands at much higher energies than the emission lines. Only in the case of the excitation spectrum of Pb^{2+} were we able to observe the mirror-symmetry band of the emission.

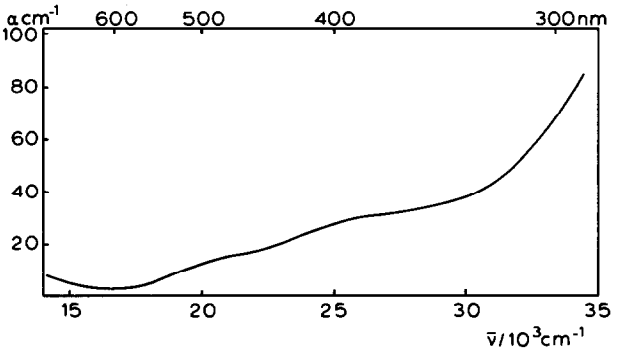

FIG. 1. Absorption spectrum of a LiH–Sb crystal at 80K.

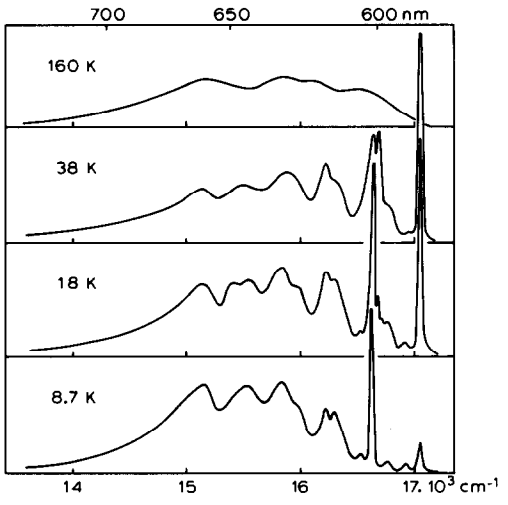

FIG. 2. Emission spectra of a LiH–Ge crystal as a function of temperature. Excitation wavelength was 450 nm.

At higher temperatures the vibrational structure disappeared. Pronounced temperature quenching of the luminescence was not observed for any of the luminescent centers under study. It is impossible to give even an estimate of the quantum efficiency of the crystals. The overall luminescence intensity was weak to medium. It is not clear what the role of the additional absorption is.

The starting dopant metal concentration was about 1 wt%. The concentration of the dopant metal ions in the LiH crystals was considerably lower, especially in the case of lead. Representative values are: LiH–Bi 2000 ppm and LiH–Pb about 50 ppm. These concentrations were determined by mass spectroscopy and X-ray fluorescence.

3.1. LiH–Ge^{2+}

Figure 2 shows the emission spectra of LiH–Ge^{2+} at different temperatures under visible excitation. Figure 3 shows the excitation spectrum of this emission at LHeT. The former spectrum is temperature dependent. The latter is not. In Table I we tabulated the emission spectrum.

The emission spectrum is an example of what was called above a narrow emission. At LHeT there is a clear, intense origin followed by some broader, vibronic lines. At higher temperatures another origin appears at 410 cm^{-1} higher energy. By plotting the logarithm of the intensity ratio of the two origins versus the reciprocal temperature we observed an activation energy of 30 cm^{-1} for the higher-energy origin. Note that this is a considerably smaller value than the spectroscopical difference between the two origins.

Decay time measurements revealed the following. The decay curves are not purely exponential, because they tend to have long tails. They could be approximated by an ex-

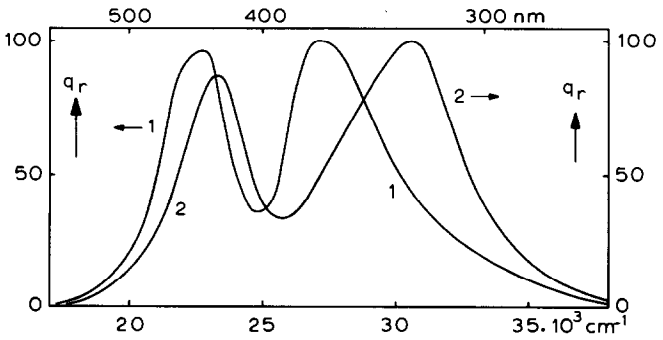

FIG. 3. Excitation spectra of the emission of a LiH–Ge crystal (1) and of a LiH–Sn crystal (2) at 4.2K. q_r gives the relative quantum output. Both curves were monitored for 640-nm emission.

TABLE I

VIBRATIONAL STRUCTURE OF THE EMISSION OF LiH–Ge (ALL VALUES IN cm^{-1}; SEE TEXT)

LHeT	Higher temp.	Assignment
Visible excitation		
	17,050	0–0′
	16,760	ν_5 (290)
	16,680	ν_2 (370)
16,640		0–0
16,290		ν_5 (350)
16,220		ν_2 (420)
+ lines under uv exc.		
Ultraviolet excitation		
16,325 (br)		0–0
15,920 (br)		ν_2
15,580 (br)		$2\nu_2$
15,150 (br)		$3\nu_2$
		ν_2 (ave.) = 390

ponential for a certain time after the pulse (Fig. 4). Decay times derived from these exponentials are given in Fig. 5. Note their strong temperature dependence in a temperature region where the total emission intensity is constant. By plotting τ similarly to the intensity ratio of the origins we derived an activation energy of 25 cm^{-1}, in good agreement with the intensity ratio measurements.

Under ultraviolet excitation we could excite a broader emission band with an equidistant number of vibronic lines (see Table I).

3.2. *LiH–Sn^{2+}*

The results for LiH–Sn^{2+} are very similar to those mentioned above for LiH–Ge^{2+}. Figure 6 presents the emission spectra as a function of temperature. In Table II the emission spectrum is tabulated. The difference between the two origins is 390 cm^{-1}. The activation energy from the intensity ratio is only 60 cm^{-1}. The excitation spectrum is given in Fig. 3, and the decay times are plotted in Fig. 5. From this figure we derive a value of 55 cm^{-1} for the activation energy.

3.3. *LiH–Sb^{3+}*

The case of LiH–Sb^{3+} is different from those of LiH–Ge^{2+} and LiH–Sn^{2+}. The emission spectrum is given in Fig. 7, together with the excitation spectrum. The emission spectrum shows vibrational structure. The lines are equidistant (400 cm^{-1}), forming a progression. There is no striking

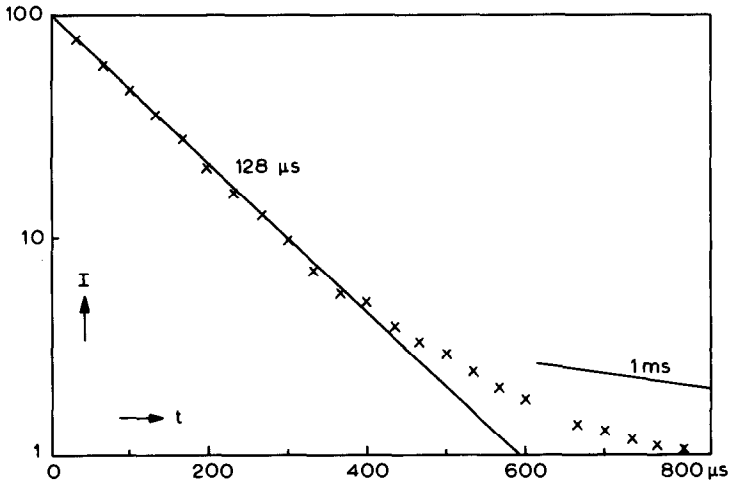

FIG. 4. Decay curve for the emission of LiH–Ge at 4.2K. Broadband ultraviolet excitation. The 1-msec slope is discussed in the text.

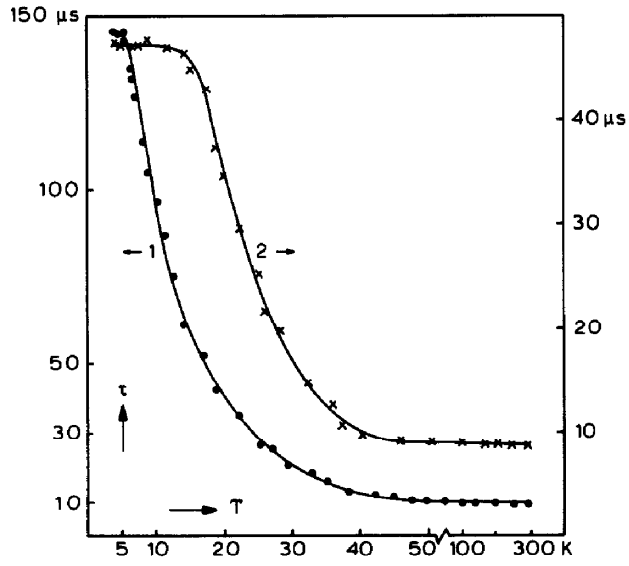

FIG. 5. Decay times as a function of temperature for the emission of LiH–Ge (1) and LiH–Sn (2). Note break in temperature scale.

temperature dependence, apart from the fact that the vibrational structure disappears above 70K. The decay time of this luminescence at LHeT was 25 μsec and becomes shorter at higher temperatures.

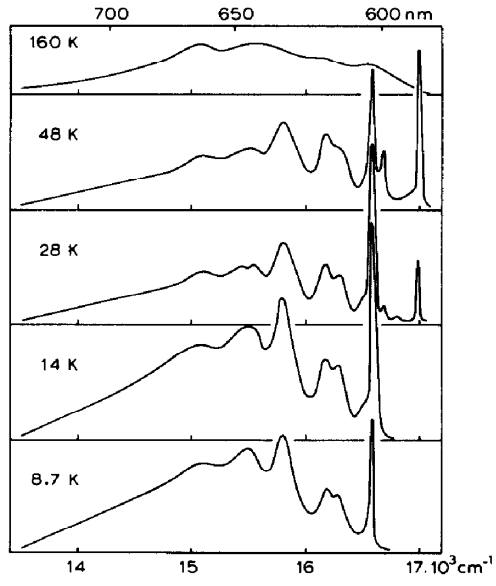

FIG. 6. Emission spectra of a LiH–Sn crystal as a function of temperature. Excitation wavelength was 450 nm.

3.4. *LiH–Pb²⁺*

The case of LiH–Pb^{2+} is by far the most complicated. Figure 8 presents several

TABLE II

VIBRATIONAL STRUCTURE OF THE EMISSION OF LiH–Sn (ALL VALUES IN cm^{-1}; SEE TEXT)

LHeT	Higher temp.	Assignment
Visible excitation		
	16,990	0–0′
	16,680	ν_5 (310)
16,600	16,600	0–0, ν_2 (310)
16,290		ν_5 (310)
16,180		ν_2 (420)
15,800		$2\nu_2$
+ lines under uv exc.		
Ultraviolet excitation		
~16,240		0–0
~15,800		ν_2
~15,400		$2\nu_2$
~15,040		$3\nu_2$
		ν_2 (ave.) = 380

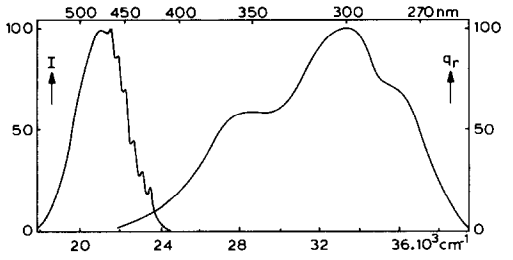

FIG. 7. Emission (left) and excitation (right) spectra of the luminescence of LiH–Sb at 4.2K. The excitation wavelength was 320 nm; the emission wavelength monitored 520 nm.

emission spectra. Dependent on excitation wavelength we find two different emission spectra at LHeT. One is similar to that of LiH–Sb^{3+}, the other to those of LiH–Ge^{2+} and LiH–Sn^{2+}. The latter is strongly temperature dependent. At higher temperatures another origin (b) appears, not at higher, but at lower energy than the low-temperature origin a. At still higher temperatures, however, another line (c) appears in between these lines (see Fig. 8). The emission spectra are tabulated in Table III. The

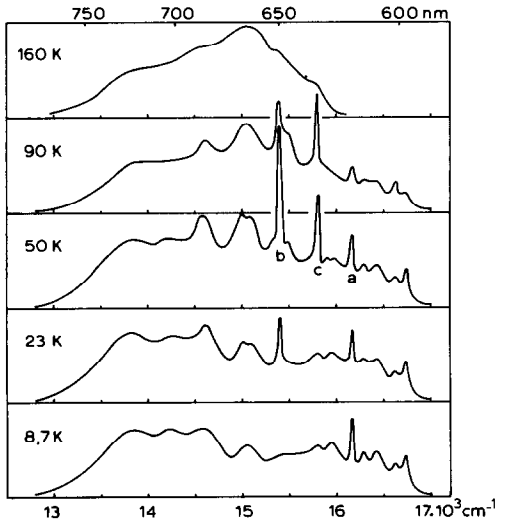

FIG. 8. Emission spectra of a LiH–Pb crystal as a function of temperature. Excitation wavelength was 550 nm. The letters a, b, and c refer to the text and Table III.

TABLE III

VIBRATIONAL STRUCTURE OF THE EMISSION OF LiH–Pb (ALL VALUES IN cm^{-1}; SEE TEXT. a, b, AND c REFER TO FIG. 8)

LHeT	Higher temp.	Still higher temp.	Assignment
	Visible excitation		
16,740			
16,610			} Other centers
16,420			
16,280			
16,170 (a)			0–0′ (T)
15,960 (br)			?
		15,805 (c)	0–0′ (X)
15,790			0–0′ (T)–ν_2 (380)
		~15,485	0–0′ (X)–ν_5 (320)
		~15,405	0–0′ (X)–ν_2 (400)
	15,395 (b)		0–0 (X)
	15,075		0–0 (X)–ν_5 (320)
		~15,005	0–0′ (X)–$2\nu_2$
	14,990		0–0 (X)–ν_2 (405)
	14,590		0–0 (X)–$2\nu_2$
	+ lines under uv exc.		
	Ultraviolet excitation		
15,000			0–0
14,600			ν_2 (400)
14,200			$2\nu_2$
13,800			$3\nu_2$

temperature dependence of the intensity ratio of the lines yields an activation energy of 25 cm^{-1} for the one appearing at the lowest temperature (b), and 115 cm^{-1} for the one appearing at a still higher temperature (c) (relative to b). The behavior of the lines b and c reminds of LiH–Ge^{2+} and LiH–Sn^{2+}.

The other emission spectrum is not strikingly temperature dependent. It consists of a number of equidistant vibronic lines (400 cm^{-1}), the fourth member of the progression being the most intense one.

The relevant excitation spectra are given in Fig. 9. Note that in this case we were able to observe some vibronic lines on the low-energy side of the excitation spectrum. The lowest one coincides with the origin a in emission. The others are at 120, 270, and 440 cm^{-1} from the origin in the excitation spectrum. A similar excitation spectrum has been reported by Rebane *et al.* (*8*).

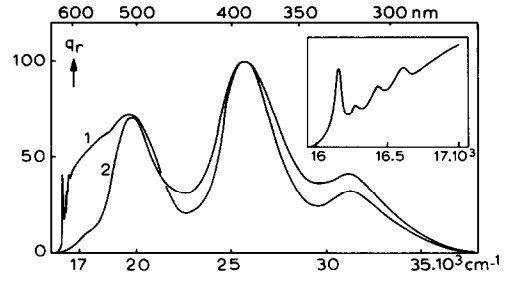

FIG. 9. Excitation spectra of the luminescence of LiH–Pb at 4.2K. Curve 1 is for 660-nm emission and curve 2 for 730-nm emission. The inset illustrates the vibrational structure in curve 1.

In emission we also observed some weak lines at energies higher than origin a. In view of the fact that at LHeT the excitation spectrum starts with line a, these additional emission lines are ascribed to different centers. This part of the emission spectrum varied from crystal to crystal. In one crystal we found a clear origin at LHeT at 16,890 cm^{-1}. This line was also observed by the authors of Ref. (*7*), who reported a large number of lines at energies higher than origin a.

Decay time measurements did not yield conclusive results. In view of the relative weakness of the emission we had to observe the total emission intensity, so that we measure the decay of a large number of centers. The curves are by no means exponential. In the temperature region where line c appears a considerable shortening of the decay is observed, comparable to the situation for LiH–Ge^{2+} and LiH–Sn^{2+}.

3.5. *LiH–Bi^{3+}*

The emission and excitation spectra of LiH–Bi^{3+} are comparable to those of LiH–Sb^{3+}. The emission and excitation spectra of LiH–Bi^{3+} are given in Fig. 10. The progression frequency in the emission spectrum is 425 cm^{-1}. The vibrational structure disappears above 60K. The decay time of the emission at LHeT is about 35 μsec and becomes shorter at higher temperatures.

3.6. *Undoped LiH*

In all samples we observed another emission which was also observed in undoped LiH. Figure 11 gives the emission and excitation spectra of this luminescence. Its intensity does not vary with temperature up till 300K. Since the optical band gap of LiH is situated at about 250 nm (*9*), this emission cannot be intrinsic. If the cryostat was opened to bring the crystal in contact with air, the intensity of this luminescence had increased when the measurement was repeated. We therefore assume that this luminescence is due to atmospheric attack of LiH at the surface. Its decay time was about 5 msec at LHeT and 1 msec at 80K. None of the emissions mentioned above

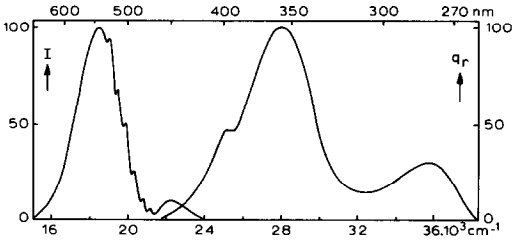

FIG. 10. Emission (left) and excitation (right) spectra of the luminescence of LiH–Bi at 4.2K. The excitation wavelength was 348 nm, the emission wavelength monitored 600 nm. The weak emission band at 450 nm is also observed for undoped LiH (compare Fig. 11).

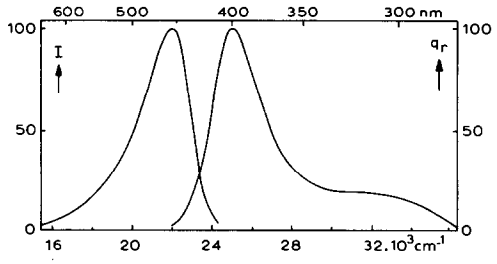

FIG. 11. Emission (left) and excitation (right) spectra of the luminescence of an undoped LiH crystal at 4.2K. The excitation wavelength was 360 nm, the emission wavelength monitored 500 nm.

were observed in the undoped LiH. In all the experiments mentioned above special care was taken to reduce to a minimum the atmospheric attack of freshly cleaved LiH crystals.

Infrared spectra of undoped LiH crystals showed an absorption peak at about 3670 cm^{-1}. The intensity of this peak increased slowly with time if the crystal was left in the air.

4. Discussion

It seems obvious to ascribe the emission transitions of the crystals under study to transitions on the s^2 ions. The present results are, however, more complicated than those observed for the other host lattices with rock salt structure. Only for the trivalent ions (Sb^{3+} and Bi^{3+}) do we observe one type of emission, but for the divalent ions there are at least two different types of emission, viz., one which reminds one of that of the trivalent ions and one which is much narrower. It is hard to separate these two emissions spectrally, so we do not have excitation spectra of the two different centers at our disposal.

Since the trivalent ions have a twofold effective, positive charge in LiH, we assume that the broad emissions are due to an s^2 ion associated with a charge compensator. This may be $V_{Li}^{\prime}$ or $O_H^{\prime}$. The narrow emissions, observed only for the divalent ions, are then ascribed to an s^2 ion without charge compensation. Therefore we will try to analyze our data as follows. First the narrow spectra will be discussed in terms of $^3P_{1,0} \rightarrow {}^1S_0$ emission transitions in a MH_6^{4-} octahedron. The broad spectra will be discussed later.

4.1. *LiH–Ge^{2+} and LiH–Sn^{2+}*

The sharp line at 16,640 cm^{-1} (LiH–Ge^{2+}) and at 16,600 cm^{-1} (LiH–Sn^{2+}) dominates the emission spectrum at LHeT under visible excitation. This is assumed to be the origin of the $^3A_{1u} \rightarrow {}^1A_{1g}$ ($^3P_0 \rightarrow {}^1S_0$) emission. It is followed by some vibronic lines, the longer wavelength part of which is covered by the broad emission which can be excited selectively in the ultraviolet. These vibronics are given in Tables I and II; their assignment will be discussed below. At higher temperatures another set of lines appears as shown in Tables I and II. They also contain a clear origin, viz., at 17,050 cm^{-1} (LiH–Ge^{2+}) and at 16,990 cm^{-1} (LiH–Sn^{2+}). This is ascribed to the pure electronic $^3T_{1u} \rightarrow {}^1A_{1g}$ ($^3P_1 \rightarrow {}^1S_0$) transition. These also carry a restricted number of vibronic lines. This interpretation runs parallel with that for s^2 ions in the alkaline earth oxides (*4–6*).

Since the $^3A_{1u} \rightarrow {}^1A_{1g}$ transition is completely forbidden, the origin is a false origin only. This explains why the energy difference between the $^3A_{1u}$ and the $^3T_{1u}$ level from the spectra (~400 cm^{-1}) differs from that derived from the temperature dependence (~30 and 60 cm^{-1}). The latter value is the real energy difference between $^3A_{1u}$ and $^3T_{1u}$. As expected it is larger for Sn^{2+} than for Ge^{2+}. The former value is about 360 cm^{-1} higher. This is the frequency of the phonon which makes the $^3A_{1u} \rightarrow {}^1A_{1g}$ transition possible. It should have T_{1g} symmetry (*4*). Since the false origin of $^3A_{1u} \rightarrow {}^1A_{1g}$ and the pure origin of $^3T_{1u} \rightarrow {}^1A_{1g}$ are both allowed, they should carry the same vibronic lines. This agrees with our results.

From the decay time measurements it follows that the low-temperature $^3A_{1u} \rightarrow {}^1A_{1g}$ emission has a considerably longer lifetime than the thermally occupied $^3T_{1u} \rightarrow {}^1A_{1g}$. The activation energy should equal the 30 and 60 cm^{-1} mentioned above and this is actually observed. The lifetimes, however, are about one order of magnitude shorter than expected, because transitions of the type $^3P_0 = {}^1S_0$ are known to have radiative transition probabilities of about 10^3 sec^{-1} (*4–6*). Our shorter values cannot

be due to nonradiative losses in the excited ions. The parabolae offset must be small in view of the vibrational structure with its short progression. This makes nonradiative transitions rather improbable (*12*). We ascribe the observed short values to energy transfer to the centers responsible for the absorption in the region where the luminescent centers emit. If this would be correct, the radiative decay time would equal the slope of the decay curve after long times. This slope tends to values of the order of a millisecond as indicated in Fig. 4 for comparison. This is the value to be expected.

If this interpretation is correct the present spectra are the first example of Ge^{2+} and Sn^{2+} emission bands with vibrational structure. Let us now turn to the narrow emission spectra of LiH–Pb^{2+}.

4.2. *LiH–Pb^{2+}*

In the case of LiH–Pb^{2+} we were able to measure an excitation spectrum which shows a clear zero-phonon line, in agreement with the previous work (*8*). This line coincides with one of the origins in the emission spectra, viz., the 16,170-cm^{-1} line. This observation leaves only one assignment, viz., a transition of the type $^3P_1 \rightarrow {}^1S_0$. This is the only allowed transition. We note that it is hard to find a series of vibronics around this line. As far as they are present, they are rather weak.

The absence of the corresponding $^3P_0$ emission may be due to the fact that a large $^3P_1$–$^3P_0$ energy difference cannot be bridged by the lattice phonons (*6*). In fact this difference is expected to be large for small-offset cases (*13*). One might argue that the line at 15,395 cm^{-1} which appears at higher temperatures is due to this line. This, however, does not give the assignment of the 15,805-cm^{-1} line which occurs at even higher temperatures. In fact the missing $^3P_0$–$^1S_0$ emission is expected at even lower energies, viz., about 14,500 cm^{-1} ($^3P_1$–$^3P_0$ distance > 1000 cm^{-1}), and this is the region which is covered by the broad emission band.

For the explanation of the 15,395- and 15,805-cm^{-1} bands we have to look for another mechanism. In view of the low lead concentration, thermally activated energy transfer to another center seems unlikely. We feel that our observation is related to the fact that in the alkali halides two emission bands are also observed. This has been explained by the presence of two minima on the APES of the $^3T_{1u}$ relaxed excited state (*1–3*). The 15,395-cm^{-1} line is then ascribed to $^3A_{1u} \rightarrow {}^1A_{1g}$ emission from the X minimum and the 15,805-cm^{-1} line to $^3T_{1u} \rightarrow {}^1A_{1g}$ emission from the X minimum. The 16,170-cm^{-1} emission is then due to emission from the T minimum. Note that the X lines carry more pronounced vibronics than the T line. The assignment is given in Table III.

The difference between LiH–Ge^{2+} and LiH–Sn^{2+} on one hand and LiH–Pb^{2+} on the other is the presence of the T line in the case of lead. The X lines are completely similar to the emission lines observed for tin and germanium. The activation energy observed between the X lines is, therefore, the trap depth of the X minimum. This increases with increasing principal quantum number. The activation energy observed for the 15,395-cm^{-1} emission corresponds to the barrier height between the T and the X minimum. The fact that the X minimum becomes more pronounced in the sequence $6s^2 \rightarrow 4s^2$ is in agreement with existing theories (*1–3*).

Let us now turn to the assignment of the vibronics. Generally speaking we observe two vibrational frequencies, viz., about 400 cm^{-1} and about 320 cm^{-1}. There is a tendency to form a progression on the 400-cm^{-1} frequency. This is a little obscured by the coincidence that the energy difference between the true origin of the $^3T_{1u} \rightarrow {}^1A_{1g}$ transition and the false origin of the $^3A_{1u} \rightarrow$

$^1A_{1g}$ transition is also about 400 cm^{-1}. Since the progressions are only observed for X emissions, the 400-cm^{-1} frequency is ascribed to the internal ν_2 mode of the MH_6^{4-} octahedron. More extended progressions built upon ν_2 have been observed for the emission from the X minimum in the case of Cs_2MX_6 (M = Se, Te; X = Cl, Br) (*14*). Note that for Pb^{2+} in the alkaline earth oxides a progression in ν_1 is observed, but this is emission from a single minimum on the APES. The 320-cm^{-1} mode is then necessarily the ν_5 mode of the octahedron in view of symmetry arguments (*6*). Its value is relatively high, but this may be due to the fact that light particles (H^-) are involved.

The situation in the case of lead is additionally complicated by a number of weaker lines at energies below the 16,170-cm^{-1} origin. These lines vary from crystal to crystal. In view of the fact that the 16,170 cm^{-1} occurs as origin in emission as well as in excitation, these additional lines are assigned to other Pb^{2+} centers. It should be kept in mind that the Pb^{2+} ion (1.19 Å) is much larger than the Li^+ ion (0.76 Å). Here we use the Shannon radii (*15*). This may result in association with the charge-compensating lithium vacancies. Since this is possible in at least two ways (along [100] and along [110]), several additional centers may result. For LiH–Sn^{2+} these additional lines were hardly detectable, for LiH–Ge^{2+} they were not detectable. The Ge^{2+} radius (0.73 Å) is nearly equal to that of Li^+.

If this would be correct, the broad emission spectra must be ascribed to another type of center. The associate $(M^{2+}–O^{2-})^x$ seems to be an obvious possibility.

Decay times of LiH–Pb^{2+} are not very informative. This is not surprising, since the number of transitions in the total emission is large. Therefore we did not analyze the decay times any further.

It is interesting to note in this connection that the $^1S_0 \rightarrow {}^3P_1$ absorption of Pb^{2+} in alkali iodides is a very narrow band (e.g., for LiI–Pb^{2+} at 77K the half-width is about 500 cm^{-1}) (*16*). For CdI_2–Pb^{2+} even narrower spectra were reported for this transition (*17*). This compares with the situation for LiH–Pb^{2+}. It is interesting that for CdI_2–Pb^{2+} a broader emission band is also observed at lower energies than the narrow one. This may well be a Pb^{2+}–O^{2-} emission, since oxygen seems to be an obvious impurity in CdI_2 crystals.

In our broad emission bands we observe a progression in about 400 cm^{-1} (see Tables I–III). This may indicate that the broad emissions are A_X emissions with vibrational structure which can be assigned to a progression in ν_2.

The strong bands in the excitation spectra of the emissions discussed are probably not related to the emission transitions. Apart from the origin in the case of LiH–Pb^{2+} they do not show any mirror symmetry to the emission spectra. The more obvious assignments are transitions of the A-band type ($^1S_0$–$^1P_1$) and charge-transfer transitions. For Pb^{2+} in iodides (*16*) the latter transitions are observed just below 5 eV. In the even more covalent hydride they will be situated at lower energy.

Let us now turn to the trivalent ions.

4.3. *LiH–Bi^{3+} and LiH–Sb^{3+}*

Although Pb^{2+} and Bi^{3+} have very similar spectra in CaO (*4–6*), they are different in LiH. Since the broad emission bands show a progression in about 400 cm^{-1}, we assign this emission to A_X emission. In view of the analogy with the longer-wavelength emissions in the case of the divalent ions, the relevant center may well be $(Bi^{3+}–2O^{2-})^x$. Similar reasonings are valid for the case of Sb^{3+}. The decay times are even shorter than for the divalent metal ions. This may be due to the fact that these emissions are at shorter wavelengths and overlap with a region of stronger absorption of our crystals.

4.4. *Undoped LiH*

Lithium hydride reacts readily with the atmospheric surroundings. The reaction products may be Li_2O, LiOH, and Li_2CO_3 (*18*). To assign the luminescence observed for undoped LiH (Fig. 11), we made a comparison with other oxygen centers in alkali halides. The O^{2-} ion in alkali halides is known to absorb in the ultraviolet region, but does not luminesce (*19*). Another center in alkali halides is the O_2^- radical. It has been studied by several authors (*20*). Its luminescence exists up to 200K. The emission spectrum shows extended vibrational structure and has a large Stokes shift (*21*) relative to the excitation band. This makes it unlikely that the emission of Fig. 11 is due to O_2^- centers.

The OH^- ion has been reported to luminesce, even at room temperature, in a spectral region which is not very different from that in Fig. 11 in a large number of compounds. Examples are KBr–OH^- (*22, 23*), NaOH and KOH solutions (*24*), and OH^- on alumina (*25*) and on MgO (*26*). We therefore propose to assign the spectra in Fig. 11 to the OH^- ion. From the present data it cannot be decided whether this is OH^- in LiOH or in LiH (or both). The value of the decay time of this emission agrees with that reported in the literature for OH^- emission (*23*). Further, the presence of a peak at 3670 cm^{-1} in the infrared spectrum is clear evidence for the presence of OH^- groups in or on our crystals.

5. Conclusion

The metal ions with s^2 configuration seem to offer highly interesting luminescent properties when incorporated in lithium hydride. They show vibrational structure which is contrary to the situation in the alkali halides but similar to that in the alkaline earth oxides. Further, they show A_T as well as A_X emission. We feel, however, that the present study does not really prove the models proposed. The problem with our crystals seems to be that they contain a certain amount of other centers which make luminescent measurements difficult. Up till now we did not succeed in improving this situation. For the future it seems tempting to try to obtain pure, s^2-ion-activated LiH crystals in order to study the luminescence in more detail. This, however, is a very heavy preparative challenge.

Acknowledgments

The authors are indebted to Dr. Inkeri Yliruokanen (Helsinki University of Technology) for the performance of the chemical analysis of some crystals, to Drs. V. Pustovarov, T. Betenekova, and N. Zavjalov (Sverdlovsk) for the growth of the single crystals, and to Dr. C. W. M. Timmermans for experimental advice in the measurements.

References

1. A. Fukuda, *Phys. Rev. B* **1,** 4161 (1970).
2. A. Fukuda, A. Matsushima, and S. Masunaga, *J. Lumin.* **12/13,** 139 (1976).
3. S. Masunaga, N. Goto, A. Matsushima, and A. Fukuda, *J. Phys. Soc. Japan* **43,** 2013 (1977).
4. A. E. Hughes and G. P. Pells, *Phys. Status Solidi A* **25,** 437 (1974); and *B* **71,** 707 (1975).
5. A. F. Ellervee, *Phys. Status Solidi B* **82,** 91 (1977).
6. A. C. van der Steen and L. T. F. Dycks, *Phys. Status Solidi B* **104,** 283 (1981).
7. L. Rebane, F. Gavrilov, B. Pirogov, S. O. Cholakh, S. Somov, G. Pilipenko, and B. Shulgin, *Izv. Akad. Nauk Est. SSR Fiz. Mat.* **20,** 483 (1971).
8. L. A. Rebane, B. V. Vlasov, F. F. Gavrilov, S. O. Cholakh, and V. D. Pirogov, *Opt. Spectrosc.* **35,** 91 (1973).
9. V. G. Plekhanov, G. S. Zavt, T. A. Betenekova, A. A. O'Connel-Bronin, and S. O. Cholakh, *Solid State Commun.* **25,** 159 (1978).
10. G. S. Zavt, K. A. Kalder, I. L. Kuusmann, Ch. B. Lushchik, V. G. Plekhanov, S. O. Cholakh, and R. A. Evarestov, *Fiz. Tverd. Tela* **18,** 2722 (1976); *Izv. AN SSSR Ser. Fiz.* **40,** 1914 (1976).
11. H. Ronde and G. Blasse, *J. Inorg. Nucl. Chem.* **40,** 215 (1978).

12. See, e.g., G. Blasse, *in* "Radiationless Processes" (B. Di Bartolo, Ed.), p. 287, Plenum, New York (1980).
13. G. Blasse and A. C. van der Steen, *Solid State Commun.* **31,** 993 (1979).
14. R. Wernicke, H. Kupka, W. Ensslin, and H. H. Schmidtke, *Chem. Phys.* **47,** 235 (1980).
15. R. D. Shannon, *Acta Crystallogr. Sect. A* **32,** 751 (1976).
16. S. Hashimoto and Y. Ohiwa, *J. Phys. Soc. Japan* **48,** 1655 (1980).
17. T. Goto and M. Ueta, *J. Phys. Soc. Japan* **29,** 1512 (1970).
18. See, e.g., "Comprehensive Inorganic Chemistry" (J. C. Bailer, Jr., H. J. Emeléus, R. Nyholm, and A. F. Trotman-Dickenson, Eds.), Vol. 1, p. 344, Pergamon, Oxford (1975).
19. F. Fischer, H. Gründig, and R. Hilsch, *Z. Phys.* **189,** 79 (1966).
20. H. R. Zeller and W. Känzig, *Helv. Phys. Acta* **40,** 845 (1967).
21. J. Rolfe, *J. Chem. Phys.* **40,** 1664 (1964); *Phys. Rev.* **123,** 447 (1961).
22. D. A. Patterson and M. N. Kabler, *Solid State Commun.* **3,** 75 (1965); H. Kostlin, *Solid State Commun.* **3,** 81 (1965).
23. H. J. Maria and S. R. McGlynn, *J. Chem. Phys.* **52,** 3402 (1970).
24. P. B. Merkel and W. H. Hamill, *J. Chem. Phys.* **55,** 2174 (1971).
25. M. Breysse, G. Coudurier, B. Claudel, and L. Faure, *J. Lumin.* **26,** 239 (1982).
26. S. Coluccia, M. Deane, and A. J. Tench, "Sixth International Conference on Catalysis, London," paper A9 (1976).